Angularly-Resolved 3D Foliage Modeling and Measurements at 60 and 80 GHz: From Stochastic Geometry to Deterministic Channel Characterization

Jiri Blumenstein*, Radek Zavorka*, Josef Vychodil*, Tomas Mikulasek*, Jarosław Wojtuń‡, Jan M. Kelner‡, Cezary Ziółkowski‡, Rajeev Shukla†, Markus Hofer§, Thomas Zemen§, Christoph F Mecklenbrauker‖, Aniruddha Chandra†, Ales Prokes*

‡Institute of Communications Systems, Military University of Technology, Warsaw, *Poland*; †ECE Department, National Institute of Technology, Durgapur, *India*; §AIT Austrian Institute of Technology, Vienna, *Austria*; ‖Institute of Telecommunications, TU Wien, Vienna, *Austria*; *Brno University of Technology, Brno, *Czechia*

***Abstract*—In this paper, we show a stochastic approach to generate a 3D model of a foliage, which is then used for deterministic ray-tracing channel modeling. This approach is verified by a measurement campaign at 60 and 80 GHz with 2 GHz bandwidth. The wireless channel is characterized by path-loss and RMS delay spread and we show the angular dependency of those parameters when the receiver is placed on a half-circle around the tree. Besides electromagnetic material properties, the 3D model is characterized by several interpretable parameters, including tree volume, leaf size, leaf density, and the tree crown shape parameter.**

***Index Terms*—ray-tracing, channel modeling, channel sounding, millimeter waves.**

I. Introduction

The millimeter-wave band, spanning the electromagnetic spectrum from 30 to 300 GHz, offers extraordinary bandwidth and, consequently, high potential data rates. It is also well known that path loss is a function of frequency. Compared to lower frequencies, millimeter-wave channels thus exhibit a higher path loss. However, this can be compensated for by utilizing higher-order antenna arrays with the same physical area as antennas operating at lower frequencies [1]. The more problematic part of the millimeter-wave band is a low diffraction contribution and high penetration losses [2]. Thus, in this paper we concentrate on the problematic situations when the line-of-sight (LOS) is obstructed by vegetation and only the reflection and/or the diffraction contributions are available (please see Fig. 1 and 2).

Either derived heuristically, from measurement datasets or from geometrical representations, various channel modeling techniques have been explored in the literature [3], but a complete review of all the modeling methods exceeds the scope of this paper. Instead, we concentrate on deterministic methods, particularly ray-tracing-based site-specific channel modeling, which offers interpretable and visualizable channel state information (CSI) [4].

Let us note that the accuracy of the derived CSI heavily relies on the precision of the 3D environment models used [5]. This reliance is especially critical at millimeter-wave frequencies, where the wavelength is in the millimeter range, rendering even minor environmental details vital for model accuracy.

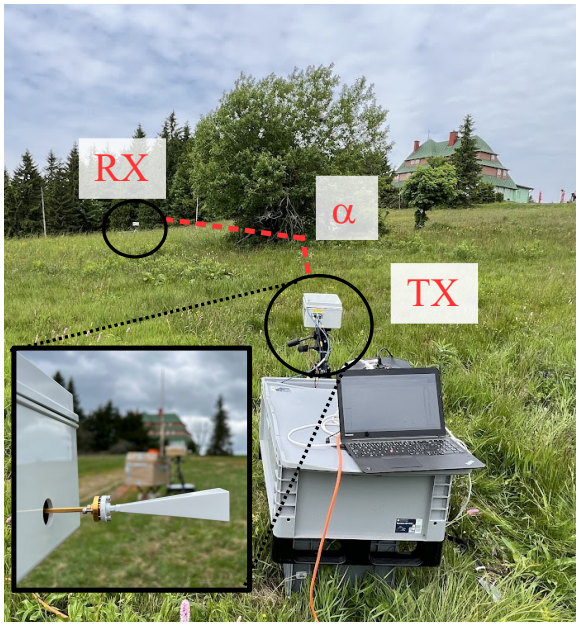

Fig. 1: Photo of the 60 and 80 GHz channel sounder. The receiver (RX) is located on the left side from the measured foliage. The distance from the TX to the tree and from the tree to the RX is 15 m.

A method for 3D foliage modeling presented in [6] utilizes hollow geometric shapes to represent trees and foliage. This approach applies extra attenuation depending on the distance rays traverse through foliage blocks.

Similarly, in [7], trees are modeled as hollow cubic forms, with the outer foliage shape (the envelope) significantly simplified. For wide-band signals with high spatial resolution, the lack of ray interactions within the foliage volume may lead to unwanted artifacts in the channel impulse responses (CIRs). Thus, in [8], the cubic volume is divided into voxels, whereas in [9], trees are represented by canopy and trunk, each

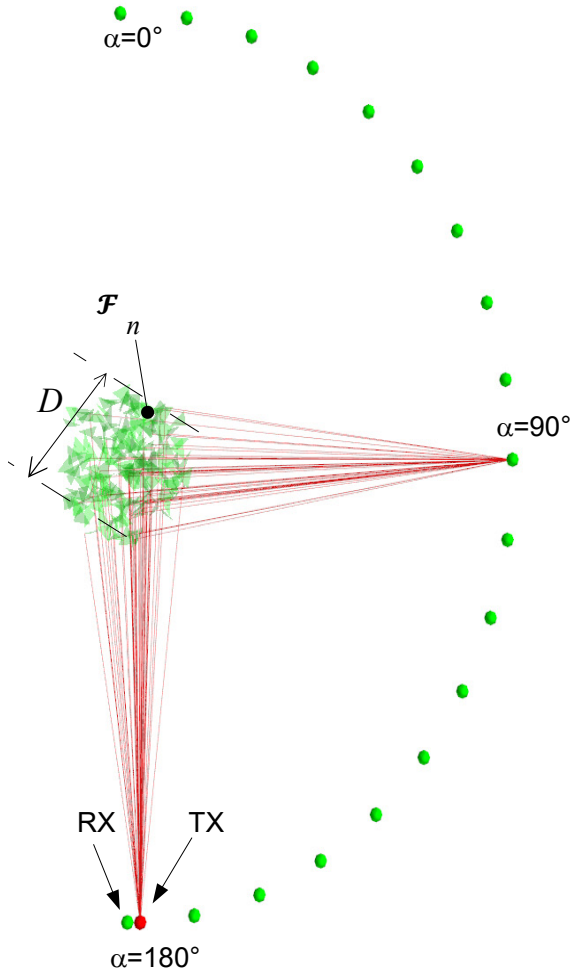

Fig. 2: Top-down view on the ray-tracing scenario depicting the half-circular placement of receivers. For clarity, we depict rays only for $\alpha = 90°$. D stands for three crown diameter and the triangular element $\mathcal{F}_n$ represents n-th face. Please note that the LOS is suppressed and not visualized. We assume isotropic radiation. The transmitter is slightingly moved sideways to allow for visualization.

modeled as concentric cylinders. In [10], vegetation scattering is represented through a hybrid approach combining physics-based modeling with data-driven elements. The foliage is described as a dielectric slab populated with randomly oriented leaves (modeled as disks) and branches (modeled as cylinders), which contribute to both scattering and attenuation of the electromagnetic field. In [11], scattering within vegetation is instead approximated by placing point scatterers inside a tree volume, typically defined by simple geometric shapes such as spheres or cylinders.

In [12], the authors employ point scatterers to model roadside scattering elements. These scatterers are treated as infinitesimal points, lacking physical thickness or randomized orientation—unlike actual leaves in a natural tree. This abstraction limits the physical realism of the model and affects both the visualization and interpretability of ray-tracing results.

In this paper, we present a methodology for the generation of the 3D foliage model and subsequent ray-tracing simulation. The fundamentals of this approach are described in [13] and in [14] we provide in-depth details of the measurement campaigns including the description of the channel sounders. The contribution of this paper is as follows:

- Results of angularly-resolved simulations of the path-loss and root mean square (RMS) delay spread of a wireless propagation through a foliage.
- Comparison and validation of the simulated and measured channels at 60 and 80 GHz with 2 GHz bandwidth.

II. Stochastic 3D Foliage Modeling Methodology

The 3D model consists of vertices, where each triplet of vertices forms a triangular face. A set of these triangular faces represents scattering objects that are randomly positioned and oriented within a predefined area - we can view this as a tree crown envelope. Such a cloud of randomly placed and rotated scattering faces serves as an input for the ray-tracing simulation. In the following section, we provide a more rigorous description of the 3D model generation process.

A. Creation of the 3D foliage model

The basis for modeling the shape (envelope) of the tree crown is a pair of sets, the set of vertices $\mathcal{V}'$ and the set of faces $\mathcal{F}'$. We write:

$$\Gamma' = (\mathcal{V}', \mathcal{F}'), \quad \text{where } \mathcal{V}' \subset \mathbb{R}^3. \tag{1}$$

Specifically, the set of vertex positions is written as:

$$\mathcal{V}' = \{\mathbf{v'}_1, \mathbf{v'}_2, \ldots, \mathbf{v'}_{3M}\}, \quad \mathbf{v'}_i \in \mathbb{R}^3 \tag{2}$$

and the set of triangular surfaces is given by:

$$\mathcal{F}' = \{\mathcal{F}'_1, \mathcal{F}'_2, \ldots, \mathcal{F}'_M\}, \tag{3}$$

where M is the number of triangles.

For simplicity, we assume that each vertex lies on the unit sphere, $\|\mathbf{v}_i\| \approx 1$. To obtain the irregular shape of the tree crown, we utilize a point-wise deformation function $P : \mathcal{V}' \to \mathcal{V}$, which deforms the initial shape Γ' by adding a random displacement $\boldsymbol{\delta}_i$ sampled from a 3D normal distribution. The vertices are then given as:

$$\mathbf{v}_i = \mathbf{v'}_i + \boldsymbol{\delta}_i, \quad \boldsymbol{\delta}_i \sim \mathcal{N}(\mathbf{0}, \xi^2\mathbf{I}), \tag{4}$$

where ξ is a user-defined parameter controlling the deformation strength.

In order to set the volume of the tree crown, we determine the ratio of the desired volume V_D and the initial volume V_I as: $\sigma = \left(\frac{V_\mathrm{D}}{V_I}\right)^{1/3}$. Then, the vertices are scaled according: $\mathbf{v}_i^\mathrm{D} = \sigma \cdot \mathbf{v}_i$. With this scaling operation we ensure that the resulting shape $\Gamma = (\{\mathbf{v}_1^\mathrm{final}, \mathbf{v}_2^\mathrm{final}, \ldots, \mathbf{v}_N^\mathrm{final}\}, \mathcal{F}')$ approximately matches the desired volume of the tree crown.

At this stage, the tree crown is ready to be filled with scattering triangular faces $\mathcal{F} \subset \mathbb{N}^3$, creating an stochastic internal structure of the foliage. Each $\mathcal{F}$ is defined in a local

coordinate system centered at the origin and its vertices are written as:

$$\mathbf{p}_1 = \left(0, -\frac{l}{\sqrt{3}}, 0\right), \mathbf{p}_2 = \left(\frac{l}{2}, \frac{l}{2\sqrt{3}}, 0\right), \mathbf{p}_3 = \left(-\frac{l}{2}, \frac{l}{2\sqrt{3}}, 0\right) \tag{5}$$

where $l = \sqrt{\frac{4A}{\sqrt{3}}}$ is the side length of the equilateral triangle with user-defined area A, representing the actual scattering face. The next step is that each face is randomly rotated utilizing a Rodrigues' rotation matrix $\mathbf{R} \in \mathbb{R}^3$.

The triangles $\mathcal{F}$ are defined by local coordinates $\mathbf{p}_j \in \mathbb{R}^3$ (for $j = 1, 2, 3$), and their rotated counterparts are defined as:

$$\mathbf{p}'_j = \mathbf{R} \cdot \mathbf{p}_j. \tag{6}$$

In the next step, the rotated triangular face is translated to a random position $\mathbf{s}_j$ utilizing a random offset $\mathbf{c} \in \mathbb{R}^3$ such that $\mathbf{c} \sim \mathcal{U}(\Gamma)$ and $\mathbf{c} \in \Gamma$. Here, $\mathcal{U}(\Gamma)$ denotes a uniform distribution within Γ, meaning that every point within the volume has the same probability of occurrence. Now, the rotated and translated vertices are given as:

$$\mathbf{s}_{i1} = \mathbf{c}_i + \mathbf{R} \cdot \mathbf{p}_1, \quad \mathbf{s}_{i2} = \mathbf{c}_i + \mathbf{R} \cdot \mathbf{p}_2, \quad \mathbf{s}_{i3} = \mathbf{c}_i + \mathbf{R} \cdot \mathbf{p}_3 \tag{7}$$

This process of filling the envelope Γ could be repeated in order to satisfy the density of the faces ρ.

III. Ray-tracing and measurements

In this section we describe both ways of gathering data from the measurement campaign and from the subsequent ray-tracing simulations.

A. Ray-tracing

The ray-tracing simulation of wireless propagation through the 3D foliage model is performed using the open-source ray tracer Sionna, version 1.0.2 [15]. The material parameter settings are based on the ITU-R P.833 recommendation [16]. We use a scattering coefficient $\mu_s = 0.50$, relative permittivity of $\epsilon_r = 17$ and conductivity $\kappa = 0.05$ S/m. Utilizing the pulse-shaping, we reduce the bandwidth (BW) to 2 GHz. Table I lists the 3D model parameters.

As for the computational cost, the model consisted of hundreds of triangles/faces which is the main factor determining the computational duration. In the presented cases, the simulation took milliseconds on a regular office laptop with a Ryzen 5 processor and without a dedicated GPU.

Parameter	Description
A [m^2]	Area of each internal triangle
V_D [m^3]	Target volume of the outer shape
ξ[$-$]	Perturbation strength (standard deviation of noise)
ρ [triangles/m^3]	Internal triangle density
r_seed [$-$]	Random seed (optional, for reproducibility)

TABLE I: Table of user-defined parameters for the tree-crown shape generation and internal triangle placement.

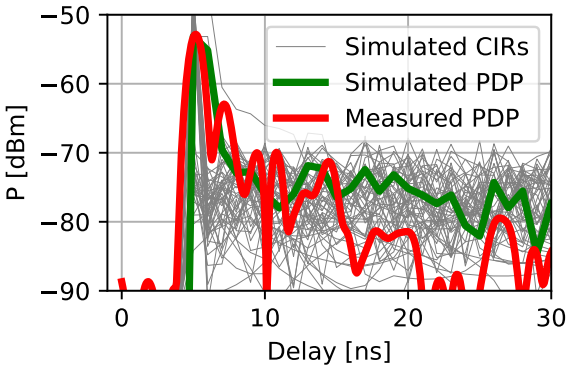

Fig. 3: Measured and ray-traced PDPs and CIRs (in absolute value squared) for $\alpha = 0°$ at 80 GHz. We generate twenty random 3D foliage realizations for the given tree crown parameters.

B. Measurement campaign

The measurement environment is depicted in Fig. 1, where we see the tree under test. It is a deciduous tree with rather small leaves (4-5 cm of length) that is measured during the summer. The transmitter (TX) is located 15 m in front of the tree and its horn antenna with 24.8 dBi gain is always pointed towards the tree and parallel to the ground. The same holds for the RX, which was moved around the tree on a half-circular trajectory, while its horn antenna with 24.8 dBi gain is also parallel to the ground and pointed towards the tree.

In [14], the outline of the RX and TX measurement positions is provided. For the verification of the ray-tracing outcome, we utilize the positions RX2 at $\alpha = 180°$ and RX4 at $\alpha = 105°$. For the RX4 location, the LOS component was removed from the measured data at the post-processing stage. The reason for the removal is that the LOS component does not interact with the tree for most RX positions as they are not hidden behind the tree, thus it carries no information on the tree.

C. Measurement and ray-tracing simulation comparison

In Fig. 3 we compare the measured and simulated PDPs at $\alpha = 0°$ and 80 GHz. Here we note that the aim of this methodology is not a photorealistic recreation of the tree and subsequent exact CSI determination. The aim is a stochastic 3D modeling technique parametrized with physically meaningful parameters, which is used for deterministic and explainable ray-tracing. With that in mind, a qualitative assessment based on visual inspection indicates that the simulation closely matches the measured data.

In Fig. 4 we compare cumulative distribution functions (CDFs) for both 60 and 80 GHz. We simulate 20 random realizations of a tree with the density $\rho \in \{0.05, 0.25\}$, perturbation strength $\xi = 0.1$ (i.e. almost circular tree-crown shape), $V_\mathrm{D} = 600\,\mathrm{m}^3$ and $A = 2\,\mathrm{m}^2$. The area of each triangle is notably larger than that of a real-world leaf. However, it

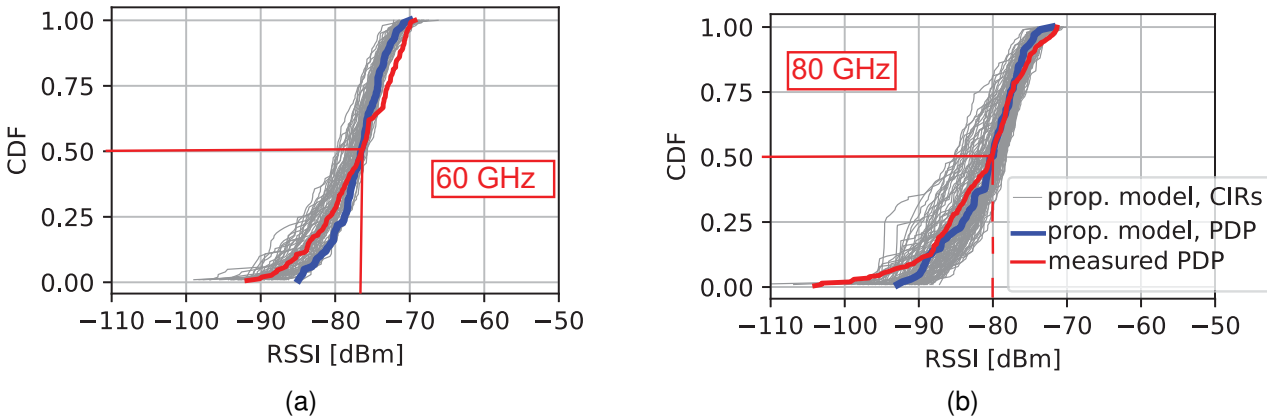

Fig. 4: CDF evaluation of the simulated and measured PDPs for (a) at 60 GHz and (b) at 80 GHz for $\alpha = 105°$. Here, the tree crown density was varied such that $\rho \in \{0.05, 0.25\}$. Please note that the subfigures (a) and (b) share the same legend.

was determined by simulation that reducing the triangle size does not significantly improve the match with measurements. Therefore, the largest triangle area that still provides a good fit to the measurements was used.

In Fig. 4 (a) we see the CDFs of the two frequency bands examined, that are the 60 and 80 GHz. As for the 60 GHz band, in Fig. 4 (a) we read that 50% of received signal strength indicator (RSSI) values is -77 dBm or less. In the case of 80 GHz in Fig. 4 (b), we read that 50% is RSSI values are -80 dBm or less. The difference between the 60 and 80 GHz is that the 60 GHz band has approximately 3 dB lower attenuation, when propagating through a tree. Here it is interesting to remind, that free-space path loss (FSPL) is 2 dB lower for the 60 GHz band than for the 80 GHz.

D. Angularly-resolved RMS delay spread and path-loss

A complete description of a wireless channel is provided by the CIR, written by [17]:

$$h(t,\tau) = \sum_{n=1}^{N} G_n a_n(t,\tau)\delta(\tau - \tau_n), \tag{8}$$

where N is the number of multipath components (MPCs), a_n is the amplitude and phase of the n-th MPC. The term $\delta(\tau - \tau_n)$ represents the Dirac delta function, indicating the time delay of the multipath component n. The effects of the receiving and transmitting antennas are given in the term G_n.

Important parameters of wireless channels are the path-loss and the RMS delay spread. The path-loss simply sums all the energy in the CIR according to:

$$\mathrm{PL} = \sum_{\tau} |h(\tau)|^2, \tag{9}$$

please note that in the ray-tracing simulation, the TX power is set to $0\,\mathrm{dBm}$.

The RMS delay spread describes how strong the delay dispersion of the channel is and it is written as [17]:

$$\mathrm{DS} = \sqrt{\frac{\sum_\tau (\tau - \bar{\tau})^2 P(\tau)}{\sum_\tau P(\tau)}}, \text{where } \bar{\tau} = \frac{\sum_\tau \tau P(\tau)}{\sum_\tau P(\tau)}. \tag{10}$$

The term $P(\tau)$ represents the power-delay profile (PDP) and is given as:

$$P(\tau) = \mathbb{E}|h(\tau)|^2. \tag{11}$$

Please note that the simulations and the measurements are assumed to be time-invariant, and thus the Doppler shift is not included in the complex base-band representation of the CIR in (8) and for the same reason $P(\tau)$ depends only on τ, while t is omitted.

In Fig. 5 we can see the evaluation of the ray-tracing simulations for the case when the proposed 3D model of the foliage is orbited by the RX. The interpretation of the α angle is available in Fig. 2. For each α, we generate twenty random 3D foliage models using the same settings. Each realization is naturally different, as the tree crown shape, the positions and orientations of the scattering triangles are drawn from random distributions. Thus, in Fig. 5 we show an occurrence heatmap around the mean value of the examined RMS delay spread and path-loss.

The path-loss is highest for the direct propagation through the tree ($\alpha = 0°$). For the 60 GHz band we read -140 dB and for the 80 GHz band the PL is three to four dB higher. Please note that the LOS component, if present, would be at -100 dB at 80 GHz and -97 dB at 60 GHz for the given distance of 30 m. When we subtract the loss caused by the free space propagation, we see that the additional attenuation caused by the tree is around 20 dB at $\alpha = 180°$ and 40 dB at $\alpha = 0°$. In simulations and also in the measurements, the LOS is removed. The reason is that most of the RX locations are not behind the tree, thus the LOS is not interacting with the tree and because it is much stronger than the remaining

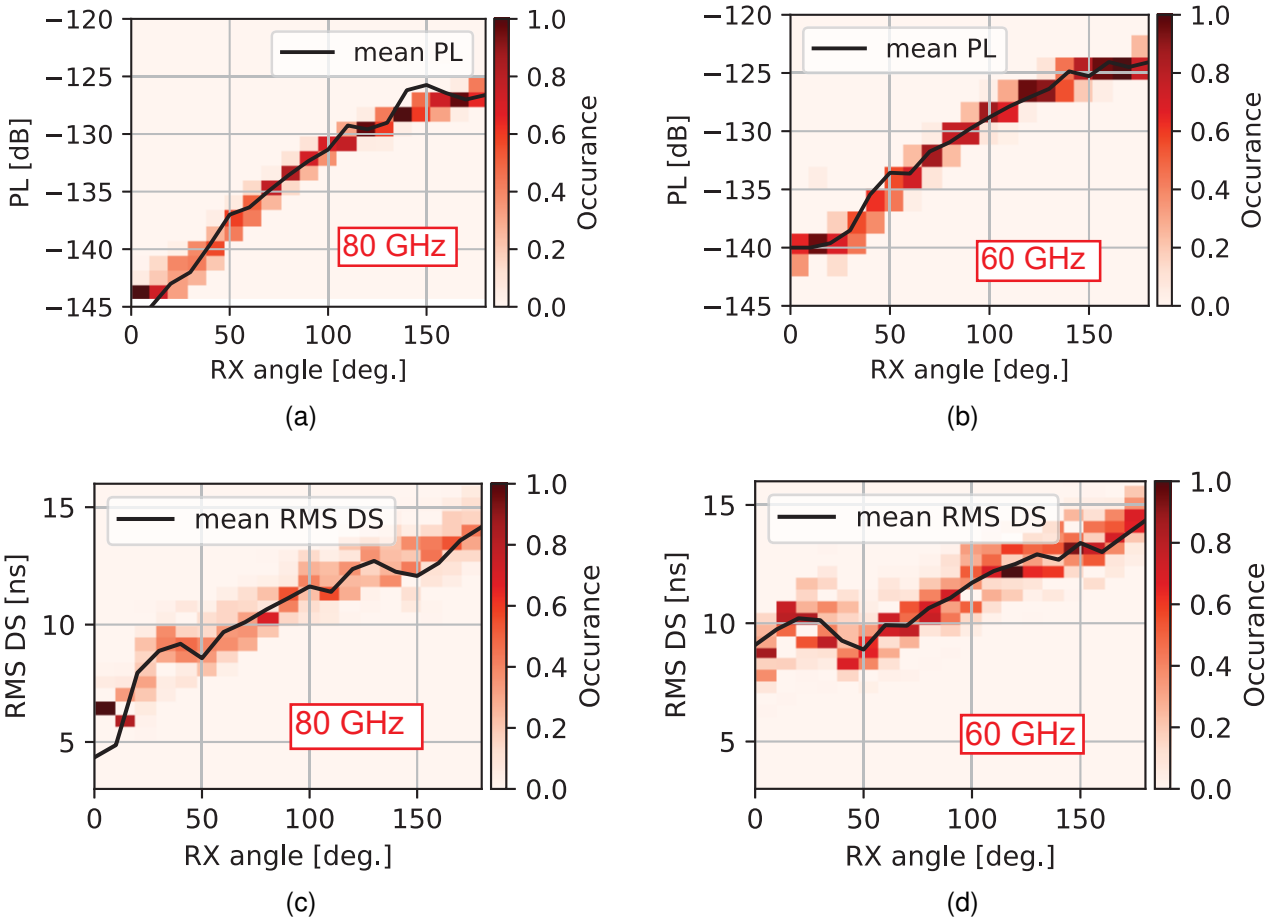

Fig. 5: The angularly resolved (a, b) path-loss and (c, d) RMS delay spread heatmaps for the 60 and 80 GHz bands. For each angle α we generated twenty random 3D realizations of the foliage with the given tree-crown parameters.

MPCs, it would undesirably influence the PL, DS and also the CDFs in Fig. 4.

As α increases, the PL almost linearly decreases and for $\alpha = 90°$ the PL mean value is 133 dB and 130 dB for 80 GHz and 60 GHz, respectively. This represents an interesting phenomenon, where the strongest MPCs reflecting back to the transmitter at $\alpha = 180°$ interact only with the first layer of scattering triangles, and are therefore less attenuated than the MPCs that have to propagate through the entire foliage in the case of $\alpha = 0°$.

The RMS delay spread occurrence heatmap is depicted in Fig. 5 (c) and (d) for 80 GHz and 60 GHz, respectively. In general, the DS ranges from 5 ns to 15 ns and as α increases, the DS almost linearly increases as well. The intuition behind this is that MPCs arriving from the direction $\alpha = 180°$ pass through the foliage back and forth when reflecting from the most distant outer layer of scattering triangles. This results in additional delay and an increased delay spread compared to the direction $\alpha = 0°$. The variance of the DS is approximately 3 ns and does not change significantly with varying α.

IV. Conclusion

In this paper we have further developed the 3D foliage modeling methodology and we have shown the angularly-resolved path-loss and RMS delay spread values. We have done this for two frequency bands, i.e. 60 GHz and 80 GHz. The ray-tracing simulation, which accepts the proposed 3D model, is done with Sionna, which is an open-source ray-tracing tool. The simulation outcome is verified by measurements done in a real-world scenario. The PL ranges from -120 dB to -140 dB depending on the angle of arrival and angle of departure. The same holds for the RMS delay spread, which ranges from 5 ns to 15 ns.

Acknowledgment

The research described in this paper was financed by the Czech Science Foundation, Project No. 23-04304L, "Multi-band prediction of millimeter-wave propagation effects for dynamic and fixed scenarios in rugged time varying environments" and by the National Science Centre, Poland, Project No. 2021/43/I/ST7/03294, through the OPUS-22 (LAP) Call in the Weave Program.

REFERENCES

[1] T. S. Rappaport, S. Sun, R. Mayzus, H. Zhao, Y. Azar, K. Wang, G. N. Wong, J. K. Schulz, M. Samimi, and F. Gutierrez, "Millimeter wave mobile communications for 5G cellular: It will work!" *IEEE Access*, vol. 1, pp. 335–349, 2013.

[2] A. F. Molisch, V. V. Ratnam, S. Han, Z. Li, S. L. H. Nguyen, L. Li, and K. Haneda, "Hybrid beamforming for massive mimo: A survey," *IEEE Communications Magazine*, vol. 55, no. 9, pp. 134–141, 2017.

[3] I. A. Hemadeh, K. Satyanarayana, M. El-Hajjar, and L. Hanzo, "Millimeter-wave communications: Physical channel models, design considerations, antenna constructions, and link-budget," *IEEE Communications Surveys Tutorials*, vol. 20, no. 2, pp. 870–913, 2018.

[4] T. Zemen, J. Gomez-Ponce, A. Chandra, M. Walter, E. Aksoy, R. He, D. Matolak, M. Kim, J.-i. Takada, S. Salous, R. Valenzuela, and A. F. Molisch, "Site-specific radio channel representation for 5G and 6G," *IEEE Communications Magazine*, pp. 1–8, 2024.

[5] M. Kleijer, G. Steinböck, B.-E. Olsson, M. Johansson, and B. Smolders, "Impact of facade details on radio propagation at 28 GHz," in *2023 17th European Conference on Antennas and Propagation (EuCAP)*, 2023, pp. 1–5.

[6] M. M. Taygur and T. F. Eibert, "Foliage modeling for urban ray-tracing simulations using satellite images," in *2021 15th European Conference on Antennas and Propagation (EuCAP)*, 2021, pp. 1–4.

[7] F. A. Rodríguez-Corbo, L. Azpilicueta, M. Celaya-Echarri, P. Lopez-Iturri, A. V. Alejos, R. M. Shubair, and F. Falcone, "Deterministic and empirical approach for millimeter-wave complex outdoor smart parking solution deployments," *Sensors*, vol. 21, no. 12, 2021.

[8] R. Charbonnier, C. Lai, T. Tenoux, D. Caudill, G. Gougeon, J. Senic, C. Gentile, Y. Corre, J. Chuang, and N. Golmie, "Calibration of ray-tracing with diffuse scattering against 28-GHz directional urban channel measurements," *IEEE Transactions on Vehicular Technology*, vol. 69, no. 12, pp. 14 264–14 276, 2020.

[9] J. C. da Silva and E. Costa, "A ray-tracing model for millimeter-wave radio propagation in dense-scatter outdoor environments," *IEEE Transactions on Antennas and Propagation*, vol. 69, no. 12, pp. 8618–8629, 2021.

[10] P. Zhang, C. Yi, B. Yang, H. Wang, C. Oestges, and X. You, "Predictive modeling of millimeter-wave vegetation-scattering effect using hybrid physics-based and data-driven approach," *IEEE Transactions on Antennas and Propagation*, vol. 70, no. 6, pp. 4056–4068, 2022.

[11] N. R. Leonor, T. R. Fernandes, M. García Sánchez, and R. F. S. Caldeirinha, "A 3-D model for millimeter-wave propagation through vegetation media using ray-tracing," *IEEE Transactions on Antennas and Propagation*, vol. 67, no. 6, pp. 4313–4318, 2019.

[12] J. Karedal, F. Tufvesson, N. Czink, A. Paier, C. Dumard, T. Zemen, C. F. Mecklenbrauker, and A. F. Molisch, "A geometry-based stochastic MIMO model for vehicle-to-vehicle communications," *IEEE Transactions on Wireless Communications*, vol. 8, no. 7, pp. 3646–3657, 2009.

[13] J. Blumenstein, R. Zavorka, J. Vychodil, T. Mikulasek, J. Wojtun, J. M. Kelner, C. Ziolkowski, R. Shukla, M. Hofer, T. Zemen, C. Mecklenbrauker, A. Chandra, and A. Prokes, "Stochastic 3D foliage modeling at 80 GHz: Experimental validation and ray tracing simulations," *IEEE Antennas and Wireless Propagation Letters*, pp. 1–5, 2025.

[14] R. Zavorka, T. Mikulasek, J. Vychodil, J. Blumenstein, A. Chandra, H. Hammoud, J. M. Kelner, C. Ziółkowski, T. Zemen, C. Mecklenbräuker, and A. Prokes, "Characterizing the 80 GHz channel in static scenarios: Diffuse reflection, scattering, and transmission through trees under varying weather conditions," *IEEE Access*, vol. 12, pp. 144 738–144 749, 2024.

[15] J. Hoydis, S. Cammerer, F. Ait Aoudia, M. Nimier-David, L. Maggi, G. Marcus, A. Vem, and A. Keller, "Sionna," 2022, https://nvlabs.github.io/sionna/.

[16] International Telecommunication Union, "Attenuation in vegetation," ITU Radiocommunication Sector, Tech. Rep. Recommendation ITU-R P.833-9, 2016, https://www.itu.int/rec/R-REC-P.833-9-201609-I/en.

[17] A. F. Molisch, *Wireless communications*. John Wiley& Sons, 2012.